



## Functionalization of SBA-15 with EDTA and its application in removing $\text{Ca}^{2+}$ and $\text{Mg}^{2+}$ ions from hard water

### *Funcionalização da SBA-15 com EDTA e sua aplicação na remoção de íons $\text{Ca}^{2+}$ e $\text{Mg}^{2+}$ de água dura*

Vanessa da Silva Bezerra Marques<sup>1</sup>; Andarair Gomes dos Santos<sup>2</sup>; Ricardo Henrique de Lima Leite<sup>3</sup>; Francisco Klebson Gomes dos Santos<sup>4</sup>

<sup>1</sup>Mestranda do Programa de Pós-Graduação em Ciência e Engenharia de Materiais, da Universidade Federal Rural do Semi-Árido, Mossoró, Rio Grande do Norte; vanessa.sirmarques@gmail.com; <sup>2</sup>Professora da Universidade Federal Rural do Semi-Árido, Mossoró, RN, +558433178200, andarair@ufersa.edu.br; <sup>3</sup>Professor da Universidade Federal Rural do Semi-Árido, Mossoró, RN, ricardoleite@ufersa.edu.br; <sup>4</sup>Professor da Universidade Federal Rural do Semi-Árido, Mossoró, RN, klebson@ufersa.edu.br

#### ARTIGO

Recebido: 20/01/2020  
Aprovado: 26/06/2020

#### Key words:

SBA-15 synthesis  
EDTA functionalization  
Adsorption  
 $\text{Ca}^{2+}$  and  $\text{Mg}^{2+}$

#### Palavras-chave:

Síntese de SBA-15  
Funcionalização de EDTA  
Adsorção  
 $\text{Ca}^{2+}$  e  $\text{Mg}^{2+}$

#### ABSTRACT

Poor management, changes in drinking parameters and drought subject many parts of the world to survival in the face of shortages of drinking water and the quality of drinking water needs to be assessed for adequate consumption. Hard water can lead to the buildup of mineral deposits in pipes and appliances that use water on a regular basis, affecting the performance and life cycle of these items. In addition, in the presence of soap, fatty acids form an insoluble precipitate with calcium ions, making foam and cleaning difficult, as well as other problems generated by the high content of  $\text{Ca}^{2+}$  and  $\text{Mg}^{2+}$  ions present in water. The goal of this paper was to study the removal of  $\text{Ca}^{2+}$  and  $\text{Mg}^{2+}$  ions using SBA-15, a mesoporous material, functionalized with ethylenediaminetetraacetic acid and compared to its pure matrix. This adsorbent was tested in  $\text{Ca}^{2+}$  and  $\text{Mg}^{2+}$  ions solution with concentration of  $250 \text{ mg.L}^{-1}$  and  $\text{pH} = 9$ , varying the temperature in  $25^\circ\text{C}$  and  $50^\circ\text{C}$ . Mesoporous materials were synthesized by hydrothermal method and characterized by TG/DTG (Thermogravimetry and Derivative Thermogravimetry), XRD (X-Ray Diffraction) and BET (Brunauer, Emmett and Teller method). Adsorption results showed removal of up to 50% of the  $\text{Ca}^{2+}$  and  $\text{Mg}^{2+}$  ions in a short time, approximately 5 min.

#### RESUMO

O mau gerenciamento, as mudanças nos parâmetros de consumo e a seca sujeitam muitas partes do mundo à sobrevivência diante da escassez de água potável e a qualidade da água potável precisa ser avaliada para um consumo adequado. A água dura pode levar ao acúmulo de depósitos minerais em tubulações e aparelhos que usam água regularmente, afetando o desempenho e o ciclo de vida desses itens. Além disso, na presença de sabão, os ácidos graxos formam um precipitado insolúvel com íons cálcio, dificultando a espuma e a limpeza, além de outros problemas gerados pelo alto conteúdo dos íons  $\text{Ca}^{2+}$  e  $\text{Mg}^{2+}$  presentes na água. O objetivo deste trabalho foi estudar a remoção dos íons  $\text{Ca}^{2+}$  e  $\text{Mg}^{2+}$  usando a SBA-15, um material mesoporoso, funcionalizado com ácido etilenodiaminotetracético e comparado à sua matriz pura. Este adsorvente foi testado em solução de íons  $\text{Ca}^{2+}$  e  $\text{Mg}^{2+}$  com concentração de  $250 \text{ mg.L}^{-1}$  e  $\text{pH} 9$ , variando a temperatura em  $25^\circ\text{C}$  e  $50^\circ\text{C}$ . Os materiais mesoporosos foram sintetizados pelo método hidrotérmico e caracterizados por TG-DTG (Termogravimetria e Termogravimetria Derivada), DRX (Difração de Raios X) e BET (método Brunauer, Emmett, Teller). Os resultados da adsorção mostraram uma remoção de até 50% dos íons  $\text{Ca}^{2+}$  e  $\text{Mg}^{2+}$  em um curto período de tempo, aproximadamente 5 min.

#### INTRODUCTION

The quality and quantity of available water resources, changes and management of consumption parameters, as well as the drought itself make many parts of the world survive in

the face of scarcity of drinking water (MARINOSKI et al., 2018). Water quality is related to various dissolved and suspended particles and impurities, as well as physical, chemical and biological characteristics (MARCAL-SILVA et



al., 2017). Among the types of drinking water, it has those with hard characteristics (high  $\text{Ca}^{2+}$  and  $\text{Mg}^{2+}$  ions content) that represent serious environmental, industrial and domestic problems (OLIVEIRA JUNIOR et al., 2016). Furthermore, in the presence of soap, fatty acids form an insoluble precipitate with leading to the formation of soap foam.

For the treatment of contaminated waters there are different techniques, such as solvent extraction, micro/ultrafiltration, sedimentation and gravity separation, flotation, precipitation, coagulation, oxidation, evaporation, distillation, reverse osmosis, adsorption, ion exchange and electro dialysis (SANTHOSH et al., 2016). Among these techniques adsorption stands out for being highly versatile and ecologically effective employed in wastewater treatment due to its easy operation, low cost and availability of a wide range of adsorbents. In addition, adsorption can also be applied for the removal of soluble and insoluble organic, inorganic and biological pollutants (SANTHOSH et al., 2016; FIORILLI et al., 2017).

New organic/inorganic mesoporous ordered structures have been widely investigated as adsorbents for waste or contaminated water treatment due to their high surface area, large and uniform pore size. However, the surface area can be easily functionalized with heteroatoms or organic groups to confer specific hydrophobicity/hydrophilicity or to introduce specific binding sites in order to achieve greater interaction (MAJDA et al., 2016; SOLTANI et al., 2017). Among the classes of mesoporous materials stand out the SBA-15 (Santa Bárbara Amorphous) (ZHAO et al., 1998), materials considered promising for application in adsorption because

they have a hexagonal array of mesoporous and uniform size with a highly ordered channel matrix. Its surface is easily functionalized with numerous organic functions without compromising the mesostructure (LUZ et al., 2010; MORITZ and GESZKE-MORITZ, 2016; FONSECA-CORREA et al., 2016; THUNYARATCHATANON et al., 2017).

In the adsorption phenomenon, ethylenediaminetetraacetic acid (EDTA) has also attracted considerable attention as adsorbent due to the formation of a strong metal-binder complex, cost effectiveness and availability. Divalent ion capture has been studied by immobilizing EDTA on some surfaces, but there is little about the applications of EDTA-SBA-15 in the removal of ions such as  $\text{Ca}^{2+}$  and  $\text{Mg}^{2+}$  (IQBAL and YUN, 2017), as well as the capture of ions. Calcium ions in EDTA functionalized mesoporous silica matrix have not been found to date. Therefore, the goal of this paper is to synthesize SBA-15 and its functionalization with EDTA to evaluate its potential as adsorbent material in the removal of  $\text{Ca}^{2+}$  and  $\text{Mg}^{2+}$  ions in aqueous solutions in finite bath. It is also made an analysis of the structural, textural and zero charge point. Finally, kinetic and thermodynamic studies were also evaluated.

## MATERIAL AND METHODS

SBA-15 mesoporous support was synthesized by the hydrothermal method, according to the methodology proposed by Zhao et al. (1998). The reagents used in the syntheses are showed in Table 1.

**Table 1.** Reagents used in the synthesis of mesoporous materials

Reagent	Manufacturer	Purity	Chemical Formula
Tetraethylorthosilicate (TEOS)	Sigma-Aldrich	98%	$\text{Si}(\text{OC}_2\text{H}_5)_4$
Pluronic P123	Sigma-Aldrich	-	$\text{HO}[\text{CH}_2\text{CH}_2]_{20}[\text{CH}_2\text{CH}_2(\text{CH}_3)\text{O}]_{70}(\text{CH}_2\text{CH}_2\text{O})_{20}\text{H}$
Hydrochloric acid	Merck	37%	HCl

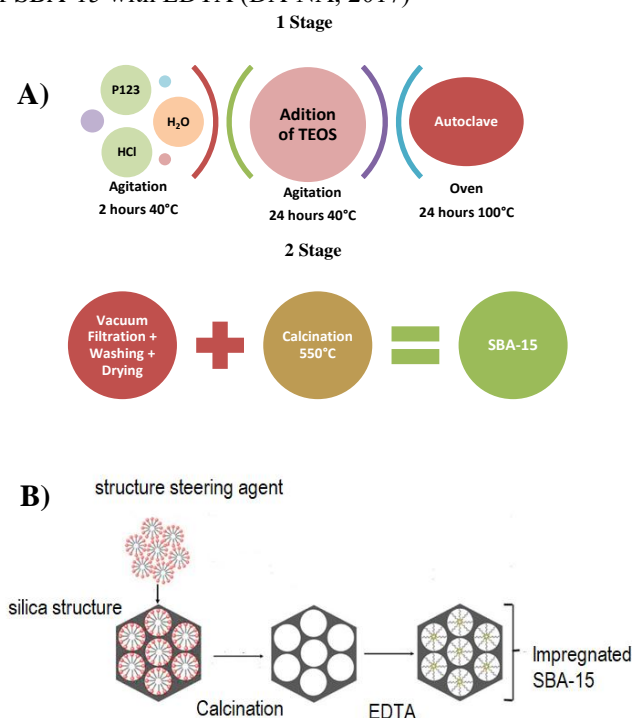
Post graft modification was applied to modify the structure of the synthesized mesoporous support and the EDTA was impregnated in the SBA-15 support by the wet spot impregnation method. In this technique a minimum volume of solution is used to cover all the dust to the point of leaving it pasty (POPA et al., 2011; DONG et al., 2013; SHENG et al., 2014). Initially, 2 mL of the EDTA solution (0.2 M) is added to 1g of SBA-15 mesoporous support then dried at 30°C for 6h. Figure 1 shows a schematic of the synthesis and impregnation process.

Table 2 summarizes a nomenclature to distinguish the synthesized materials: the SBA-15 mesoporous matrix and functionalized by wet spot impregnation.

**Table 2.** Nomenclature of synthesized mesoporous materials

Mesoporous Material	Condition	Nomenclature
SBA-15	not calcined	SBA-15 A
SBA-15	Calcinated (550°C/2h)	SBA-15 B
SBA-15	EDTA impregnated	SBA-15 C

**Figure 1.** A) Scheme of synthesis of SBA-15, B) impregnation of SBA-15 with EDTA (DA'NA, 2017)



The thermogravimetric curves (TG-DTG) of SBA-15 mesoporous support were obtained on a SHIMADZU DSC-60 and DTG-60H thermocouple with coupled DTA. For the analysis, approximately 5 mg of sample were used in alumina crucibles that were heated to 750°C, with heating rate of 10°C/min, in an inert nitrogen atmosphere. Through the thermogravimetric curves generated from the samples of non-calcined materials, it was possible to determine the amount of water and organic template present, as well as the temperature ranges in which these molecules are removed. These data are of fundamental importance in determining the lowest calcination temperature required to remove the pore director from the mesoporous support.

For the X-ray analysis of SBA-15 mesoporous materials, the powder method proposed by SETTLE (1997) was employed, which basically consists in uniformizing the sample to make it a fine and homogeneous powder. Depending on the type of material synthesized, analyzes were performed in two steps, according to the low and high angle range. In the first stage, the low angle diffractograms in the range of 0.5 to 3.0° were obtained by a Rigaku MineFlex™ II diffractometer, operating with CuK $\alpha$  radiation at 40kv, 30mA, velocity of 0.5°/min and step of 0.01deg. In a second step, the high angle diffractograms in the range of 10 to 60° were obtained by a Shimadzu model XRD - 6000 diffractometer, operating with CuK $\alpha$  radiation at 40 kv, 30mA, velocity of 0.5deg/min and step of 0.02deg (GÓMEZ et al., 2016). Structural analyzes as a function of diffractograms were characterized based on reference standards calculated from the COD database for standard chart (00-035-1779) and standard chart (00-035-1779) and using the MAUD® program. Phase Identification from Powder Diffraction Version 2.064.

The zero charge point (ZCP) is defined as the pH at which the surface of a material has a neutral charge. The methodology used for its determination is called “11-point experiment” (BARBOSA et al., 2014). 0.10 mol.L<sup>-1</sup> NaCl solutions of different pH values (ranging from 0 to 12) were prepared using distilled water at room temperature, 25°C. The pH of each solution was adjusted to the required value with HCl or NaOH solution. SBA-15 ZCP and EDTA-SBA-15 were estimated by direct pH measurements before and after contact with the solid in standard solutions (HCl/NaCl and NaOH/NaCl). Approximately 0.1g of the matrix was weighed and added in 50 mL pH adjusted solution starting from 0 to 12. The solutions were constantly stirred for 24h, and then centrifuged and the

pH of the final solution was then measured. The obtained data were represented in a graph of the pH variation ( $\Delta\text{pH} = \text{final pH} - \text{initial pH}$ ) as a function of the initial pH of the solutions with the solid. The value of the zero charge point was determined, considering  $\Delta\text{pH}$  equal to 0.

Nitrogen adsorption/desorption spectra were performed at 77K using the BET method. Each analysis contained about 0.1g of sample previously calcined which underwent a degassing process at 300°C for 10 hours. This treatment aims to remove moisture from the surface of the solid. Nitrogen adsorption isotherms for the samples were obtained in the P/P<sub>0</sub> range (approximately from 0 to 0.95), providing important information about the materials, such as: surface area, average pore diameter and pores volume. These parameters (S<sub>BET</sub>, D<sub>p</sub> and V<sub>p</sub>) were calculated using the autosorb Surface Area & Pore Size Analyzer Program® version 1.55.

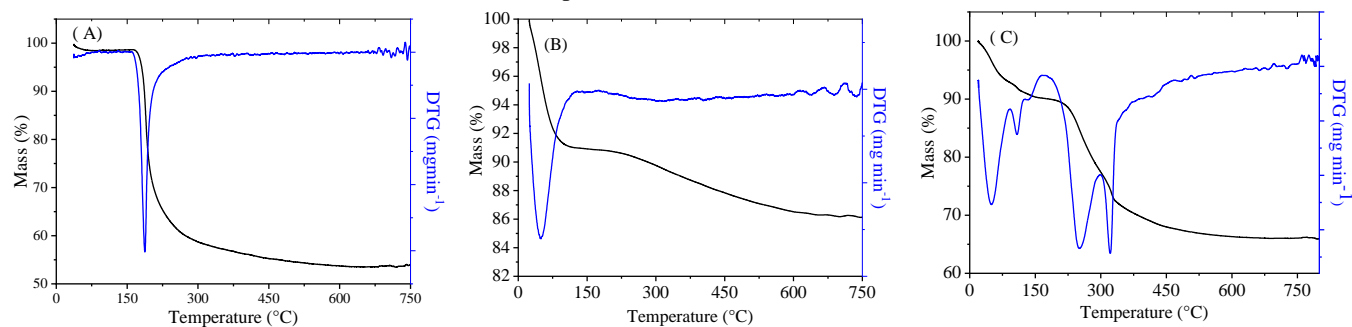
To verify the efficiency of removal of Ca<sup>2+</sup> and Mg<sup>2+</sup> ions from drinking water using the matrix SBA-15 B and SBA-15 C the adsorption experiments were performed in a finite bath. To investigate the removal rate in the pure (SBA-15 B) and impregnated (SBA-15 C) silica matrix, aqueous solutions were used at a concentration of 250 mg.L<sup>-1</sup> of CaCO<sub>3</sub> and pH=9. For each 1.0 g of adsorbent, 100 mL of the solution was used, varying the temperature and constant stirring (200 rpm). At predetermined intervals aliquots of solution were removed and filtered. The supernatant liquid was diluted and the metal concentration determined by titration.

The collected supernatants were analyzed by EDTA-Na titration method according to standard method (19th edition, 1995). To study the removal of Mg<sup>2+</sup> ions at initial concentrations of 250 mg.L<sup>-1</sup>, a 0.01 M EDTA solution was used as titrant, a pH 10 NH<sub>4</sub>Cl/NH<sub>4</sub>OH buffer solutions and the turning point Eriochrome Black T indicator from violet to blue. Whereas for the study of Ca<sup>2+</sup> ions removal in solutions with initial concentrations 250 mg.L<sup>-1</sup> a 0.01 M EDTA solution was used as titrant, pH 12 NaOH solution and the murexide indicator with pink to purple turning point. For both Ca<sup>2+</sup> and Mg<sup>2+</sup> analyzes were performed in triplicate.

## RESULTS AND DISCUSSION

Figure 2 shows TG-DTG curves for uncalcined (SBA-15 A), calcined (SBA-15 B) and EDTA impregnated (SBA-15 C) mesoporous materials, respectively.

**Figure 2.** TG-DTG (Thermogravimetry and Derivative Thermogravimetry) curves: (A) SBA-15 mesoporous matrix, (B) calcined SBA-15 B, (C) EDTA functionalized mesoporous silica (SBA-15 C)



As can be seen in Figure 2(A), the SBA-15 a TG curve (uncalcined) shows two mass losses. Such losses are related to

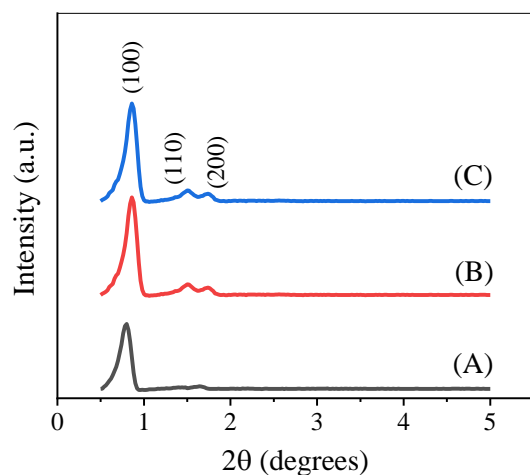
the physically adsorbed water output in the temperature range between 25°C to 100°C and the second is directly related to the

template output of the mesoporous material structure relative to the peak in the range 150°C to 200°C on the DTG curve, with 5% and 45% of mass loss, respectively. The stability of the mesoporous silica structure begins from 550°C. Analyzing Figure 2 (B) the material SBA-15 B shows a mass loss below 100°C which is attributed to water desorption. The second mass loss occurs between 200°C and 600°C due to dehydroxylation of silicate networks. According to EZZEDDINE et al., 2015, at high temperatures condensation of the silanol groups of the silica matrix is observed. For EDTA functionalized mesoporous silica (SBA-15 C), mass losses in the same temperature ranges are also observed, as shown in Figure 2 (C). However, in this case EDTA has significant mass losses in this same temperature range between 200°C and 600°C, which represents the breakdown of CN (amine) bonds corresponding to the decomposition of EDTA (SENNA et al., 2015). This can be verified by the decay in the DTG curves of Figure 2 (C), proving the impregnation of the silica matrix with EDTA (EZZEDDINE et al., 2015).

It is important to note that, as the SBA-15 support, the concept of crystallinity cannot be used, as with zeolites, because its walls are made of amorphous silica. The absence of peaks at greater angles indicates that the material is not crystalline. However, it is known that there is an orderly hexagonal network, where one pore is surrounded by six others, generating the characteristic reflection of this material. Thus, phase identification occurs when three to five peaks are observed corresponding to the planes (100), (110), (200), (210) and (300) in the range between 0.5 and 3.0°, which are according to the literature, characteristics of the hexagonal structure of the SBA-15 nanostructured mesoporous materials (GÓMEZ et al., 2016).

Figures 3 and 4 show the low and high angle diffractograms of mesoporous silica without heat treatment, calcined and impregnated with EDTA, SBA-15 A, SBA-15 B and SBA-15 C, respectively.

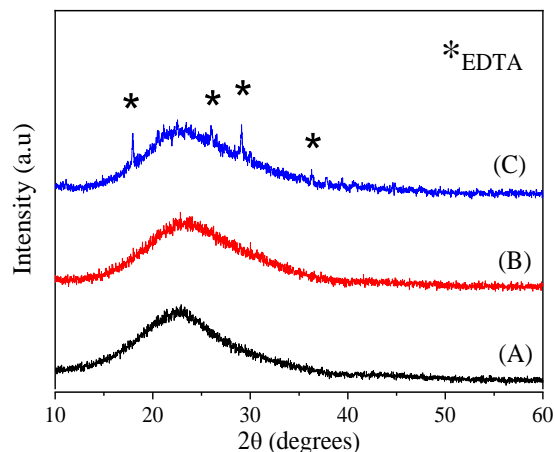
**Figure 3.** Low angle diffractograms for mesoporous silica (A) SBA-15 A; (B) SBA-15 B and (C) SBA-15 C



The diffractograms in Figure 3 show three peaks, which confirm the crystal structure of the synthesized materials. According to the powder X-ray diffraction data of the adsorbent, as illustrated in Figure 3 presents three peaks that appear in the range of  $2\theta$  between 0.5 to 2°. These peaks are indexed to the reflections (100), (110) and (200), showing that the mesoporous structure of the SBA-15 is maintained after both calcination and functionalization with EDTA. However,

the reduction in diffraction intensity reveals some degree of disorder, especially for the less intense peak attributed to organic monolayer installations within the pore structure when functionalized with EDTA as can be seen in the diffractogram of Figure 4 (C) (SBA-15-C) (WU et al., 2013).

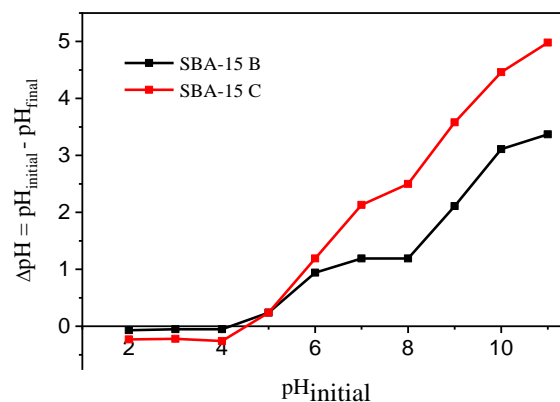
**Figure 4.** High angle diffractograms for mesoporous silica (A) SBA-15 A; (B) SBA-15 B and (C) SBA-15 C



The high angle X-ray diffraction pattern is typical of SBA-15 amorphous walls with  $2\theta$  between 20 and 25° (IQBAL and YUN, 2017) and can be observed in the three diffractograms presented. For the diffractogram for SBA-15 C (with impregnation), was attributed to peaks concerning the molecular structure of EDTA are observed, indicated by \* in Figure 4 (C). These peaks are characterized based on reference patterns calculated from the COD database for the standard chart (00-035-1779) and the standard chart (00-035-1779) and using the Phase Identification from Powder (MAUD®) program. The result presented from the molecular crystalline characterization confirms once again the presence of EDTA in the SBA-15 mesoporous silica matrix, demonstrating that the adopted wet spot impregnation technique is efficient in modifying and functionalizing the surface of the SBA-15.

The zero charge point (ZCP) is a parameter that indicates the pH value at which a given solid has a zero charge on the surface. This parameter is relevant because it allows predicting the adsorbent surface charge as a function of pH. The results found for calcined and functionalized SBA-15 are presented in Figure 5.

**Figure 5.** ZCP (Zero Charge Point) measurement experiment



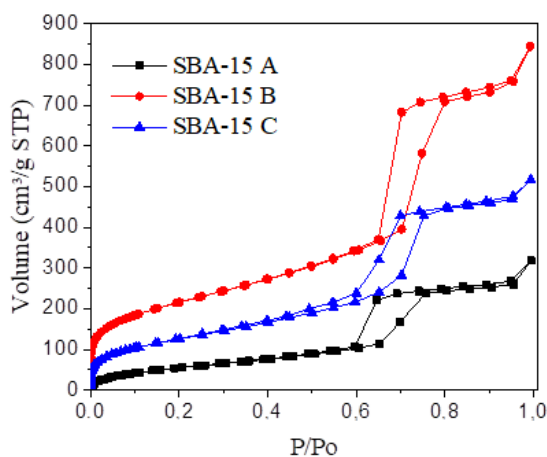
According to Figure 5, the ZCP of SBA-15 B and SBA-15 C occurs at pH 4.2 and 4.5, respectively. According to these

values, it is possible to predict the adsorbent behavior: for solution pH values lower than the ZCP value the adsorbent surface is positive (adsorbs anions) and for solution pH values greater than the ZCP, the surface charge adsorbent is negative (adsorb cations). In this case, below these values, the hydroxyls are protonated and therefore positively charged and for values above those obtained by ZCP analysis, the hydroxyls are deprotonated and negatively charged (FERREIRA and PARK, 2012).

It can be seen that SBA-15 C (functionalized) has a higher negative surface charge than SBA-15 B, showing that the impregnation with EDTA was successful, since the EDTA has coordinating oxygen and nitrogen atoms in its structure, promoting a greater number of negative active sites in the mesoporous silica matrix. In this context, the complexation reaction of calcium and magnesium atoms by EDTA is facilitated at a more alkaline pH than in most metals (eg  $\text{Zn}^{2+}$ ,  $\text{Cd}^{2+}$  and  $\text{Pb}^{2+}$ ), since at more acidic pH their complexes are less stable, being protonated EDTA instead of complexing calcium and/or magnesium (LEE et al., 2016). Thus, in order to ensure that the adsorption process occurs without the phenomenon of precipitation of  $\text{Ca}^{2+}$  and  $\text{Mg}^{2+}$  ions and the formation of stable complexes, the study was carried out at pH 9, knowing that the adsorption of cations occurs above the point. The zero-charge tests obtained were performed at this pH based on studies already carried out in the capture of calcium ions in zeolitic materials (HERRMANN and KLEIN, 1987; QIN et al., 2010a, 2010b).

Figures 6 and 7 show the 77 K nitrogen adsorption/desorption isotherms for the specific surface area obtained by the BET equation and the pore size and pore volume distribution of synthesized mesoporous materials (SBA-15 A, SBA-15 B and SBA-15 C).

**Figure 6.** SBA-15 A, SBA-15 B and SBA-15 C nitrogen adsorption/desorption isotherm



According to the IUPAC classification, type IV isotherms are observed, as shown in Figure 6. The SBA-15 A, SBA-15 B and SBA-15 C also exhibit type H1 hysteresis, characteristic of mesoporous solids (BIRTH et al., 2014). In addition, adsorption isotherms show a sharp inflection at high relative pressure ( $P/P_0 = 0.6 - 0.8$ ), which according to Dong et al., (2013) indicates typical capillary condensation within uniform pores.

**Figure 7.** SBA-15 A, SBA-15 B and SBA-15 C pore diameter distribution

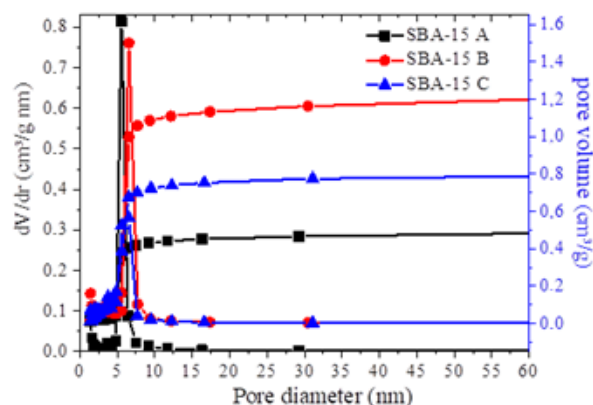


Table 3 summarizes the surface area ( $S_{BET}$ ), pore diameter ( $D_p$ ) and pore volume ( $V_p$ ) corresponding to pure SBA-15 with calcination and functionalized with EDTA (SBA-15 A, SBA-15 B and SBA-15 C, respectively).

**Table 3.** Textural characteristics for SBA-15 A, SBA-15 B and SBA-15 C

Mesoporous material	$S_{BET}$ ( $\text{m}^2/\text{g}$ )	$D_p$ (nm)	$V_p$ ( $\text{cm}^3/\text{g}$ )
SBA-15 A	197.1	5.6	0.5
SBA-15 B	744.9	6.6	1.9
SBA-15 C	435.5	6.5	1.0

As shown in Table 3, the calcined and EDTA-impregnated mesoporous material has a surface area of  $197.1 \text{ m}^2/\text{g}$ ,  $744.9 \text{ m}^2/\text{g}$  and  $435.5 \text{ m}^2/\text{g}$ , respectively. As expected, SBA-15 without calcination presents low surface area ( $197.12 \text{ m}^2/\text{g}$ ) when compared to areas of calcined SBA-15 and EDTA-functionalized SBA-15. This is due to the blockage of the pores by the organic director used in the synthesis of the silica matrix. Meanwhile, SBA-15 B (calcined) exhibits the largest surface area ( $744.9 \text{ m}^2/\text{g}$ ) even when compared to EDTA functionalized SBA-15 C ( $435.5 \text{ m}^2/\text{g}$ ). This reduction is a phenomenon also expected after mesoporous silica functionalization, which occurs due to the implantation or suspension of functional group portions inside and outside the walls of the silica structure. Functional group loading tends to decrease specific surface area and pore volume after functionalization. These functional group units block adsorption of nitrogen molecules and suppress the dew point of functionalized mesoporous silica toward lower relative pressure. Thus, it was observed a decrease in pore size and surface area after functionalization (EZZEDDINE et al., 2015).

Chong et al. (2019) synthesized SBA-15 with surface area, pore volume and pore diameter equal to  $856 \text{ m}^2/\text{g}$ ,  $0.99 \text{ cm}^3/\text{g}$  and  $7.45 \text{ nm}$ , respectively. Although it is the same synthesis method used, such variations can be attributed to the shorter drying and/or calcination time of SBA-15, 12 hours and 3 hours, respectively.

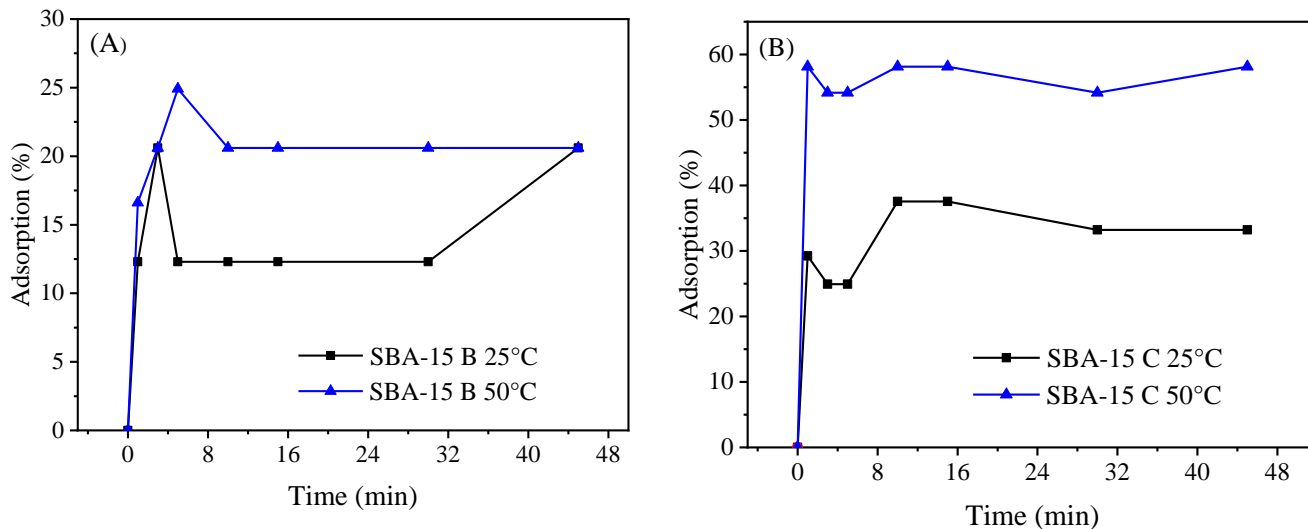
Pore and diameter volume distributions also decreased with functionalization from  $1.9 \text{ cm}^3 \text{ g}^{-1}$  and  $6.6 \text{ nm}$  (SBA-15 B) to  $1.0 \text{ cm}^3 \text{ g}^{-1}$  and  $6.5 \text{ nm}$  SBA-15 C. This behavior is also related to implantation or suspension of functional group portions within the pores of the silica thereby reducing pore volume. However, no significant changes in the shape of the mesoporous matrix are observed after functionalization and the

structure remains intact, which is in agreement with those presented by structural analysis (XRD).

Adsorption kinetics is one of the most relevant features as it represents the efficiency of the system. The effect of different contact time on the adsorption of  $\text{Ca}^{2+}$  and  $\text{Mg}^{2+}$  ions by SBA-

15 B and SBA-15 C is shown in Figures 8 to 11, respectively. The efficiency of SBA-15 as a function of temperature ( $25^\circ\text{C}$  and  $50^\circ\text{C}$ ) and pH (without pH adjustment and equal to pH 9) is presented.

**Figure 8.** Adsorption capacity of calcium ions ( $\text{Ca}^{2+}$ ) without pH adjustment: (A) SBA-15 B (B) SBA-15 C at temperatures of  $25^\circ\text{C}$  and  $50^\circ\text{C}$



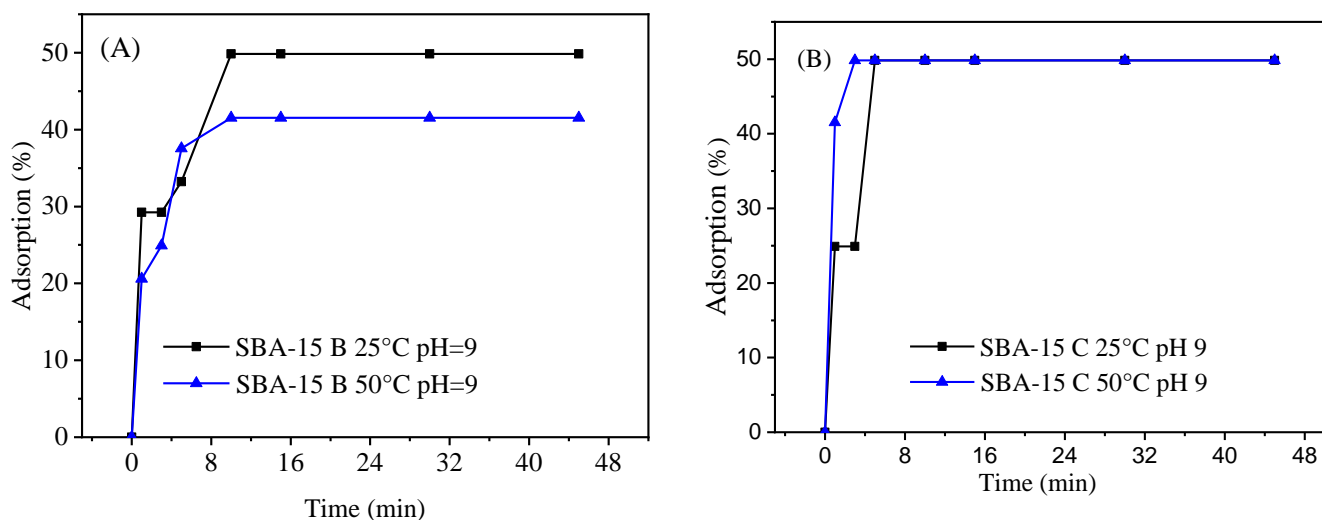
As shown in Figure 8, initially there is a significant increase in  $\text{Ca}^{2+}$  adsorption at both  $25^\circ\text{C}$  and  $50^\circ\text{C}$ . However, SBA-15 B shows a 5% increase in adsorption with increasing temperature over the same period of time. After this time, at both temperatures, there is a small reduction in adsorption, which remains constant over time, but more significant at  $25^\circ\text{C}$ , ie, a reduction of 5% at  $50^\circ\text{C}$  and 8% at  $25^\circ\text{C}$ . It can be further observed that  $\text{Ca}^{2+}$  adsorption at  $50^\circ\text{C}$  is almost 2 times higher than at  $25^\circ\text{C}$ .

When SBA-15 was functionalized with EDTA (SBA-15 C) (Figure 8b), a similar adsorption profile was observed, that

is, an increase in adsorption in the first five minutes and then remained constant over time. However, with SBA-15 C the adsorption capacity is much higher at both temperatures ( $25^\circ\text{C}$  and  $50^\circ\text{C}$ ), being more pronounced at  $50^\circ\text{C}$ , about 3 times higher when compared to SBA-15 B.

Finally, it can be concluded that in the system without pH adjustment, the temperature increase favors the adsorption of calcium ions from the medium, being a process that demands a higher energy to promote the reaction.

**Figure 9.** Adsorption capacity of calcium ions ( $\text{Ca}^{2+}$ ) at pH 9: a) SBA-15 B b) SBA-15 C at temperatures of  $25^\circ\text{C}$  and  $50^\circ\text{C}$



The profile of the  $\text{Ca}^{2+}$  ion removal curve is similar with and without the pH adjustment of the medium at 9, as shown in Figure 10. However, there is an inversion in temperature

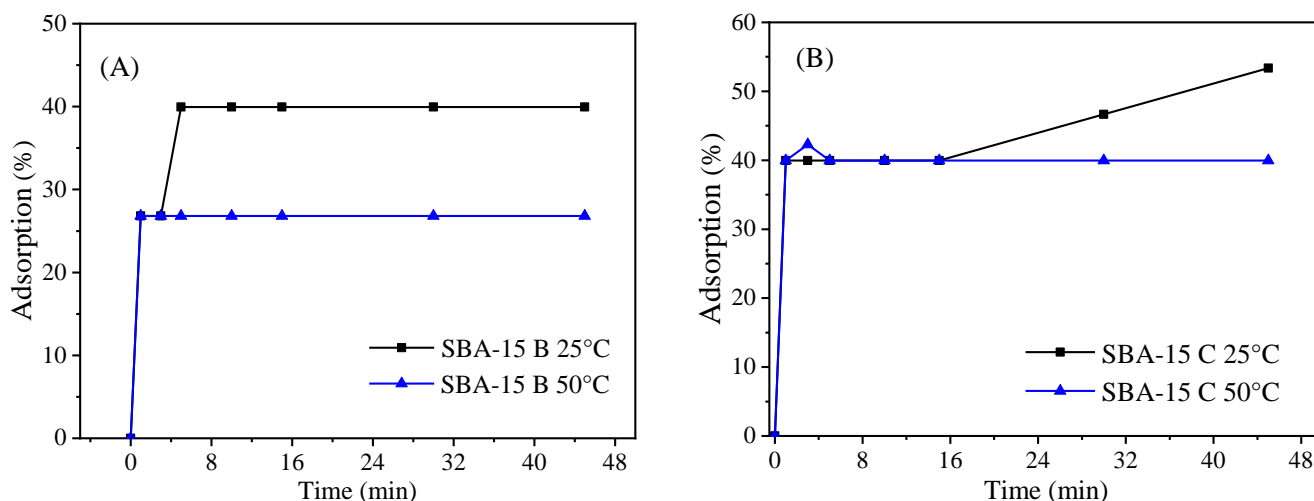
behavior with pH adjustment, ie adsorption is greater at  $25^\circ\text{C}$  than  $50^\circ\text{C}$  for SBA-15 B.

Analyzing Figures 8 (a) and 9 (a) calcined material (SBA-15 B) without pH adjustment obtained a removal rate of about

12 and 20, while at pH 9 a removal of 50 and 40% at the same temperatures, 25°C and 50°C, respectively. In this context, the pH variation favors the adsorption process of calcium ions

( $\text{Ca}^{2+}$ ) at room temperature, which proves to be a spontaneous reaction without the need to increase the medium temperature, just adjusting the pH to charge above the zero charge potential.

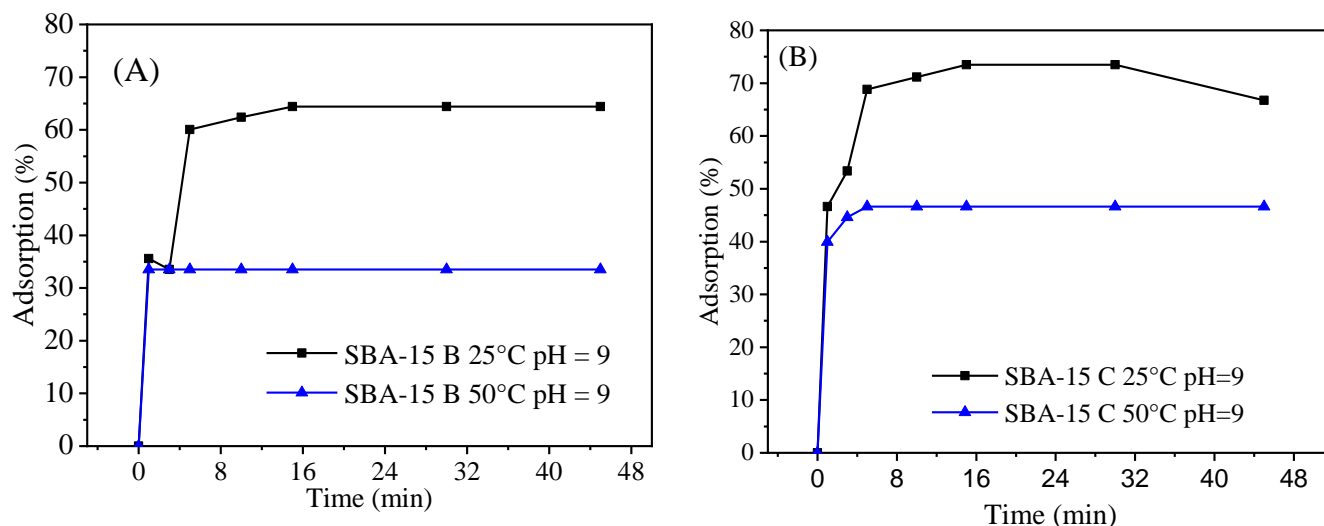
**Figure 10.** Adsorption capacity of magnesium ( $\text{Mg}^{2+}$ ) ions without pH adjustment (A) SBA-15 B, (B) SBA-15 C at temperatures of 25°C and 50°C



For the EDTA-impregnated mesoporous silica SBA-15 (SBA-15 C), a similar behavior to the previous one was observed, with an increase in the adsorption capacity, which may be justified by the presence of amine groups present in the matrix surface that contributed with the largest number of active sites for calcium ion adsorption. Removal rates were 38

and 60% for medium without pH adjustment and 50% with pH adjustment at 9 to 25°C and 50°C, respectively. When SBA-15 was functionalized with EDTA, pH adjustment did not influence the removal rate, showing that only the active sites present in the silica matrix after impregnation were sufficient to reach a high removal rate.

**Figure 11.** Adsorption capacity of magnesium ions ( $\text{Mg}^{2+}$ ) at pH 9: (A) SBA-15 B, (B) SBA-15 C at temperatures of 25°C and 50°C



Analyzing the adsorption of  $\text{Mg}^{2+}$  ions (Figure 11), the adsorption profile is similar to the  $\text{Ca}^{2+}$  ion adsorption profile with pH adjustment at 9, that is, the adsorption is higher at lower temperature: 40% and 26% for SBA-15 B and 65% and 34% for SBA-15 C at 25°C and 50°C, respectively. As well, the functionalization with EDTA promotes higher adsorption when compared to SBA-15 B. However, the adsorption capacity of magnesium ions ( $\text{Mg}^{2+}$ ) is more effective than calcium ions ( $\text{Ca}^{2+}$ ) adsorption.

This may be justified by the fact that the size of magnesium atoms is smaller than those of calcium and thus favor their migration into the pores of mesoporous silica (SBA-15), in addition to the surface bonds that are formed by the presence of active sites after EDTA impregnation. For SBA-15 B, where the medium was not modified at pH the removal rates of 40 and 26% and at pH 9 of 65 and 34% at temperatures of 25°C and 50°C, respectively.

Given these data, it is noted that the pH adjustment favors a higher adsorption rate of magnesium ions. It can also be observed that adsorption is fast for both  $\text{Ca}^{2+}$  and  $\text{Mg}^{2+}$  ions, occurring within five minutes and reaching the adsorption equilibrium within ten minutes for both SBA-15 B and SBA-15 C. Short-time adsorption rate shows that the modified SBA-15 surface has a high density of active sites. According to Ferreira and Park (2012) this is related to wet spot impregnation that does not break the mesoporous structure and functional groups being distributed around the matrix and  $\text{Ca}^{2+}$  and  $\text{Mg}^{2+}$  adsorption on the SBA-15 C support behaves as a  $\text{Ca}^{2+}/\text{Mg}^{2+}/\text{SBA-15}$  chelate.

## CONCLUSION

The heat treated or EDTA functionalized lead the SBA-15 a promising adsorbent for reducing the hardness of waste or drinking water. However EDTA functionalized SBA-15 has much higher adsorption capacity, about three times higher than heat treated SBA-15. It should also be noted that EDTA functionalized SBA-15 has higher adsorption potential regardless of pH or temperature, and the adsorption capacity of magnesium ions is about 20% higher than calcium ions adsorption under the same conditions.

## ACKNOWLEDGMENTS

The authors thank to UFERSA, the Material Characterization Laboratory (UERN) and the Advanced Materials Analysis and Synthesis Center (UFRN).

## REFERENCES

- BARBOSA, C. S.; SANTANA, S. A. A.; BEZERRA, C. W. B.; SILVA, H. A. D. S. Remoção de compostos fenólicos de soluções aquosas utilizando carvão ativado preparado a partir do aguapé (*Eichhornia crassipes*): Estudo cinético e de equilíbrio termodinâmico. *Química Nova*, v. 37, n. 3, p. 447–453, 2014. 10.5935/0100-4042.20140066
- CHONG, C. C.; THE, L. P.; SETIABUDI, H. D. Syngas production via  $\text{CO}_2$  reforming of  $\text{CH}_4$  over Ni-based SBA-15: Promotional effect of promoters (Ce, Mg, and Zr). *Materials Today Energy*, v.12, p.408-417, 2019. 10.1016/j.mtener.2019.04.001 .
- DA'NA, E. Adsorption of heavy metals on functionalized-mesoporous silica: A review. *Microporous and Mesoporous Materials*, v. 247, p. 145–157, 2017. 10.1016/j.micromeso.2017.03.050.
- DONG, B. B.; ZHANG, B. B.; WU, H. Y.; CHEN, X.; ZHANG, K.; ZHENG, X. C. Synthesis, characterization and catalytic evaluation of SBA-15 supported 12-tungstophosphoric acid mesoporous materials in the oxidation of benzaldehyde to benzoic acid. *Materials Research Bulletin*, v. 48, n. 7, p. 2491–2496, 2013. 10.1016/j.materresbull.2013.03.004 .
- EZZEDDINE, Z.; GENER, I. B.; POUILLOUX, Y.; HAMAD, H.; SAAD, Z.; KAZPARD, V. Divalent heavy metals adsorption onto different types of EDTA-modified mesoporous materials: Effectiveness and complexation rate. *Microporous and Mesoporous Materials*, v. 212, p. 125–136, 2015. 10.1016/j.micromeso.2015.03.013.
- FELLENZ, N.; ALONSO, F. J. P.; MARTIN, P. P.; FIERRO, J. L. G.; BENGUA, J. F.; MARCHETTI, S. G.; ROJAS, S. Chromium (VI) removal from water by means of adsorption-reduction at the surface of amino-functionalized MCM-41 sorbents. *Microporous and Mesoporous Materials*, v. 239, p. 138–146, 2017. 10.1016/j.micromeso.2016.10.012.
- FERREIRA, G. D.; PARK, S. W. Sílicas porosas: métodos de síntese e caracterização. Escola Politécnica da Universidade de São Paulo. Trabalho de conclusão de curso para obtenção do título de graduado em Engenharia Química, 2012.
- FIORILLI, S.; RIVOIRA, L.; CALÌ, G.; APPENDINI, M.; BRUZZONITI, M. C.; COISSON, M.; ONIDA, B. Iron oxide inside SBA-15 modified with amino groups as reusable adsorbent for highly efficient removal of glyphosate from water. *Applied Surface Science*, v. 411, p. 457–465, 2017. 10.1016/j.apsusc.2017.03.206.
- FONSECA-CORREA, R. A.; MURILO-ACEVEDO, Y. S.; GIRALDO-GUTIÉRREZ, L.; MORENO-PIRAJÁN, J. C. Microporous and Mesoporous Materials in Decontamination of Water Process. *Microporous and Mesoporous Materials*, 2016. 10.5772/64393.
- GÓMEZ, G.; BOTAS, J. A.; SERRANO, D. P.; PIZARRO, P. Hydrogen production by methane decomposition over pure silica SBA-15 materials. *Catalysis Today*, v. 277, p. 152–160, 2016. 10.1016/j.cattod.2015.12.007.
- GUO, Y.; LIU, D.; ZHAO, Y.; GONG, B.; GOU, Y.; HUANG, W. Synthesis of chitosan-functionalized MCM-41-A and its performance in Pb (II) removal from synthetic water. *Journal of the Taiwan Institute of Chemical Engineers*, v. 71, p. 537–545, 2017. 10.1016/j.jtice.2016.12.033 .
- GUZIK, A. F.; JADACH, B.; PIOTROWSKA, H.; MURIAS, M.; LULEK, J.; NOWAK, I. Synthesis and characterization of SBA-16 type mesoporous materials containing amine groups. *Microporous and Mesoporous Materials*, v. 220, p. 231–238, 2016. 10.1016/j.micromeso.2015.09.006.
- HERRMANN, C. C.; KLEIN, G. Zeolite a for selective calcium removal from brackish water? *Reactive Polymers, Ion Exchangers, Sorbents*, v. 5, n. 3, p. 281–293, 1987. 10.1016/0167-6989(87)90236-4.
- HUANG, J.; YE, MENG.; QU, Y.; CHU, L.; CHEN, R.; HE, Q.; XU, D.; Pb (II) removal from aqueous media by EDTA-modified mesoporous silica SBA-15. *Journal of Colloid and Interface Science*, v. 385, n. 1, p. 137–146, 2012. 10.1016/j.jcis.2012.06.054.
- IQBAL, S.; YUN, J.-I. EDTA-functionalized mesoporous silica for the removal of corrosion products: Adsorption studies and performance evaluation under gamma irradiation. *Microporous and Mesoporous Materials*, v. 248, p. 149–157, 2017. 10.1016/j.micromeso.2017.04.028.

- LACHOWICZ, J. I.; DELPIANO, G. R.; ZANDA D.; PILUDU, MN. ENRICO SANJUST, E.; MONDUZZI. M.; SALIS, A., Adsorption of Cu<sup>2+</sup> and Zn<sup>2+</sup> on SBA-15 mesoporous silica functionalized with triethylenetetramine chelating agent. *Journal of Environmental Chemical Engineering*, v.7, p.103205, 2019. 10.1016/j.jece.2019.103205.
- LEE, J. Y.; CHEN, C. H.; CHENG, S.; LI, H. Y. Adsorption of Pb (II) and Cu (II) metal ions on functionalized large-pore mesoporous silica. *International Journal of Environmental Science and Technology*, v. 13, n. 1, p. 65–76, 2016.
- MAJDA, D.; NAPRUSZEWSKA, B. D.; ZIMOWSKA, M. Porosity of SBA-15 after functionalization of the surface with aminosilanes. *Microporous and Mesoporous Materials*, v. 234, p. 98–106, 2016. 10.1016/j.micromeso.2016.07.013.
- MARCAL-SILVA, H.; DUARTE, F. V.; OLIVEIRA, A. L. G. Avaliação do abrandamento de água calcária utilizando hidróxido de cálcio e carbonatação. *Águas Subterrâneas*, v. 31, n. 4, p. 310-315, 2017. 10.14295/ras.v31i4.28871.
- MARINOSKI, A. K.; RUPP, R. F.; GHISI, E. Environmental benefit analysis of strategies for potable water savings in residential buildings. *Journal of Environmental Management*, v. 206, p. 28–39, 2018. 10.1016/j.jenvman.2017.10.004
- MERKACHE, R.; FECHETE, I.; MAAMACHE, M. 3D ordered mesoporous Fe-KIT-6 catalysts for methylcyclopentane (MCP) conversion and carbon dioxide (CO<sub>2</sub>) hydrogenation for energy and environmental applications. *Applied Catalysis A: General*, v. 504, p. 672–681, 2015. 10.1016/j.apcata.2015.03.032
- MESTRE, A. S.; NABIÇO, A.; FIGUEIREDO, P. L.; PINTO, M. L. Enhanced clofibrilic acid removal by activated carbons: Water hardness as a key parameter. *Chemical Engineering Journal*, v. 286, p. 538–548, 2016. 10.1016/j.cej.2015.10.066.
- MORITZ, M.; GESZKE-MORITZ, M. Amine-modified SBA-15 and MCF mesoporous molecular sieves as promising sorbents for natural antioxidant. *Modeling of caffeic acid adsorption. Materials Science and Engineering C*, v. 61, p. 411–421, 2016. 10.1016/j.msec.2015.12.093.
- OLIVEIRA JUNIOR, H. S.; SILVA, P. C. M.; SILVA, C. L. C. Monitoramento e mapeamento das águas subterrâneas de abastecimento urbano do município de Mossoró-RN. *Revista Brasileira de Geografia Física*, v. 9, p. 1825–1835, 2016. <https://doi.org/10.26848/rbgf.v9.6.p1825-1835>.
- POPA, A.; SASCA, V.; KISS, E. E.; NEDUCIN, R. M.; HOLCLAJTNER-ANTUNOVIĆ, I., Mesoporous silica directly modified by incorporation or impregnation of some heteropolyacids: Synthesis and structural characterization. *Materials Research Bulletin*, v. 46, n. 1, p. 19–25, 2011. 10.1016/j.materresbull.2010.10.003.
- QIN, C.; WANG, R.; MA, W. Characteristics of calcium adsorption by Ca-Selectivity zeolite in fixed-pH and in a range of pH. *Chemical Engineering Journal*, v. 156, n. 3, p. 540–545, 2010a. 10.1016/j.cej.2009.04.006.
- QIN, C.; WANG, R.; MA, W. Adsorption kinetic studies of calcium ions onto Ca-Selective zeolite. *Desalination*, v. 259, n. 1–3, p. 156–160, 2010b. 10.1016/j.desal.2010.04.015.
- SANTHOSH, C.; VELMURUGAN, V.; JACOB, G.; JEONG, S. K. Role of nanomaterials in water treatment applications: A review. *Chemical Engineering Journal*, v. 306, p. 1116–1137, 2016. 10.1016/j.cej.2016.08.053.
- SENNA, A. M.; BOTARO, V. R.; NOVACK, K. M. Síntese, caracterização e aplicação de hidrogel derivado de acetato de celulose e etilendiaminotetracético (EDTA) como substrato de liberação controlada de fertilizantes NPK e retenção de água em solo. 125 f. Tese (Doutorado em Engenharia de Materiais) – Escola de Minas, Universidade Federal de Ouro Preto, Ouro Preto, 2015.
- SHENG, X.; KONG, J.; ZHOU, Y.; ZHANG, Y.; ZHANG, Z. Direct synthesis, characterization and catalytic application of SBA-15 mesoporous silica with heteropolyacid incorporated into their framework. *Microporous and Mesoporous Materials*, v. 187, p. 7–13, 2014. 10.1016/j.micromeso.2013.12.007.
- SILVA, C. R. P. DA; FONSECA, E. J. DA S.; SILVA, A. O. S. Encapsulamento da Maggiferina em sílica mesoporosa: síntese e caracterização. Tese (doutorado em Materiais) - Universidade de Alagoas. Centro de Tecnologia. Programa de Pós-Graduação em Materiais, Maceió, 2017.
- SOLTANI, S.; RASHID, U.; AL-RESAYES, S. I.; NEHD, I. A. Recent progress in synthesis and surface functionalization of mesoporous acidic heterogeneous catalysts for esterification of free fatty acid feedstocks: A review. *Energy Conversion and Management*, v.141, p.183-205, 2017. 10.1016/j.enconman.2016.07.042.
- THUNYARATCHATANON, C.; LUENGNARUEMITCHAIA, A.; CHAISUWANA, T.; CHENC, S. Y.; YOSHIMURA, Y. Synthesis and characterization of Zr incorporation into highly ordered mesostructured SBA-15 material and its performance for CO<sub>2</sub> adsorption. *Microporous and Mesoporous Materials*, v. 253, p. 18–28, 2017. 10.1016/j.micromeso.2017.06.015.
- WU, L.; WANG, H.; LAN, H. Adsorption of Cu (II)–EDTA chelates on tri-ammonium-functionalized mesoporous silica from aqueous solution. *Separation and Purification Technology*, v. 117, p. 118–123, 2013. 10.1016/j.seppur.2013.06.016.
- ZHANG, K.; OSTRAT, M. L. Innovations in hierarchical zeolite synthesis. *Catalysis Today*, v. 264, p. 3–15, 2016. 10.1016/j.cattod.2015.08.012.
- ZHAO D.; FENG J.; HUO Q.; MELOSH N.; FREDRICKSON G. H.; CHMELKA B. F., STUCKY G. D. Triblock copolymer syntheses of mesoporous silica with periodic 50 to 300 angstrom pores. *Science*, v.279, n.80, p.548–552, 1998. 10.1126/science.279.5350.548.